

Journal of Biomedical Optics

BiomedicalOptics.SPIEDigitalLibrary.org

Combined ultrasound and photoacoustic imaging of blood clot during microbubble-assisted sonothrombolysis

Dhiman Das
Manojit Pramanik

SPIE.

Dhiman Das, Manojit Pramanik, "Combined ultrasound and photoacoustic imaging of blood clot during microbubble-assisted sonothrombolysis," *J. Biomed. Opt.* **24**(12), 121902 (2019),
doi: 10.1117/1.JBO.24.12.121902.

Combined ultrasound and photoacoustic imaging of blood clot during microbubble-assisted sonothrombolysis

Dhiman Das and Manojit Pramanik*

Nanyang Technological University, School of Chemical and Biomedical Engineering, Singapore

Abstract. Blockage of healthy blood vessels by blood clots can lead to serious or even life-threatening complications. The use of a combined ultrasound (US) and photoacoustic (PA) imaging was explored for blood clot monitoring during microbubble-assisted sonothrombolysis. PA imaging is an emerging hybrid imaging modality that has garnered the attention of the biomedical imaging community in recent years. It enables the study of the composition of a blood clot due to its sensitivity toward optical absorption. Here, *in vitro* imaging of the side of a blood clot facing the microbubbles was done over time. The US and PA signal-to-noise (SNR) ratio value changes during microbubble-assisted sonothrombolysis were studied for two different local environments: blood clot in deionized water and blood clot in blood. In the first case, US and PA SNR values increased by 4.6% and reduced by 20.8%, respectively after 30 min of sonothrombolysis treatment. After 10 min of sonothrombolysis treatment of the blood clot in blood, the US and PA SNR values increased by 7.7% and 38.3%, respectively. The US and PA SNR value changes were recorded in response to its local environment. This technique can be used to determine the final composition of the blood clot which may, in turn, help in the administration of clot-dissolving drugs. © The Authors. Published by SPIE under a Creative Commons Attribution 4.0 Unported License. Distribution or reproduction of this work in whole or in part requires full attribution of the original publication, including its DOI. [DOI: [10.1117/1.JBO.24.12.121902](https://doi.org/10.1117/1.JBO.24.12.121902)]

Keywords: photoacoustic imaging; ultrasound imaging; imaging systems; sonothrombolysis; microbubbles; blood clot.

Paper 190111SSR received Apr. 10, 2019; accepted for publication Jun. 12, 2019; published online Jul. 24, 2019.

1 Introduction

Blood clot, or thrombus, occurs as a response to prevent bleeding from injured blood vessels. However, these blood clots are harmful when they obstruct the blood flow through healthy blood vessels. Cardiovascular diseases such as myocardial infarction and atrial fibrillation are caused by the occlusion of blood flow through the vasculature due to the presence of blood clots or thrombi. Ischemic strokes happen when a blood clot shuts off an artery supplying blood to the brain. According to the World Health Organization,¹ an estimated 17.9 million people died from cardiovascular diseases in 2016, which represented 31% of all global deaths. Of these deaths, 85% were due to heart attack and stroke. Blood clots, or thrombi, can also cause many other life-threatening diseases,^{2,3} including pulmonary embolism (PE) in the lungs, and deep vein thrombosis (DVT) in the popliteal, femoral, or iliac veins.

Sonothrombolysis^{2,4} is a noninvasive procedure to break down blood clots using focused ultrasound (US) waves. Sonothrombolysis is shown to have higher efficiency in the presence of microbubbles⁵⁻⁷ and thrombolytic agents, such as tissue plasminogen activator.^{8,9} During clinical trials of sonothrombolysis^{10,11} for the noninvasive treatment of acute ischemic stroke, magnetic resonance imaging (MRI) and computed tomography (CT) angiography were performed to assess recanalization of the occluded blood vessels. The limitation of MRI is that it uses a strong magnetic field and cannot be used on patients with metal implants or pacemakers,¹² and it is quite expensive. With CT angiography, a contrast dye needs

to be injected into the bloodstream, which creates a risk of contrast-induced nephropathy.¹³ Other clinical studies^{14,15} used transcranial Doppler US to image the restoration of the blood flow. While US is safe, it does not provide any further information regarding the composition and age of the blood clot.¹³

It has been reported that the thrombolysis efficiency is much higher if sonothrombolysis is accompanied by clot-dissolving drugs such as tissue plasminogen activator (tPA)^{16,17} and heparin.^{18,19} Based on histopathological evaluation, it has been observed that the composition²⁰ of the thrombus is diverse. The composition²¹ depends on the volume fractions and the distribution of red blood cells (RBCs), white blood cells (WBCs), fibrin, platelets, etc. The effectiveness of clot-dissolving drugs such as tPA^{16,17} depends on the composition of the blood clot. Blood clots with higher fibrin content require a higher dosage of tPA compared to those that are rich in RBCs and WBCs. So, it will be beneficial to incorporate active diagnostic monitoring of the blood clot during sonothrombolysis.

Photoacoustic imaging (PAI)²²⁻²⁵ is a rapidly growing imaging modality. In PAI, a pulsed laser is used to excite the targeted biological tissue, which undergoes thermoelastic expansion and generates US waves. These waves are detected and recorded by an US transducer or an array of US transducers^{26,27} to form a PA image. PAI can identify a range of endogenous^{28,29} and exogenous³⁰⁻³⁵ molecules with high sensitivity. It offers unique advantages of high spatial and temporal resolution, speckle-free, and it can provide both structural and functional information using various light excitation wavelengths. As biological tissue is orders of magnitude more transparent to sound than to light in terms of scattering mean free path, PAI provides far greater depth penetration compared to pure optical imaging.²⁶ Moreover, PAI is also complementary to and compatible with

*Address all correspondence to Manojit Pramanik, E-mail: manojit@ntu.edu.sg

other imaging modalities, especially optical imaging and US imaging.²⁶

Karpiouk et al.³⁶ used combined US and PA imaging to determine the age of the blood clot. It was reported³⁶ that the amplitude of the PA signal is higher for an acute (fresh) clot compared to a chronic (long-developing) clot at 532 nm. PAI has also been demonstrated for label-free embolus detection³⁷ and for *in vivo* flow cytometry³⁸ of RBC- and WBC-rich blood clots using positive and negative contrasts in the PA signal, respectively. Blood clots need to be observed in real time during sonothrombolysis. Therefore, a dual modal US and PA imaging has been used in this work to actively monitor the blood clot. Combined US and PA imaging^{39–42} provides sufficient spatial resolution and contrast with high sensitivity and specificity in real time. While US can provide structural information such as the size and density of the clot, PA imaging can also be used to analyze other important functional parameters such as change in the RBC and WBC concentration, hemoglobin concentration, and hemoglobin oxygen saturation.

In this work, a combined US and PA imaging system is used to image a blood clot during microbubble-assisted sonothrombolysis. Microbubbles were used because they enhance the sonothrombolysis efficiency^{5–7} and are currently undergoing clinical trials.^{10,11} Moreover, microbubbles are already used as US contrast agents.⁴³ As a result, the delivery of the microbubbles to the blood clot for sonothrombolysis can be easily monitored using US imaging systems. Two cases were studied: blood clot in deionized (DI) water and blood clot in blood to gain new insights into the impact of the local environment on the blood clot. The same clot was used to observe the changes in the US and PA signal-to-noise ratio (SNR) values over time during sonothrombolysis treatment. This would be useful to monitor the changes in the composition of the blood clot and its surrounding fluids during sonothrombolysis, which may, in turn, help in adjusting the dosage of the clot-dissolving drugs^{16,17} and reduce the treatment time and its associated costs.

2 Methods

2.1 Ultrasound and Photoacoustic Imaging System

A frequency-doubled nanosecond-pulsed Nd:YAG pump laser (Continuum, Surelite Ex) was used as light excitation source for PA imaging. The pulse repetition frequency of the laser is 10 Hz and the pulse width is 5 ns in duration. A dichroic mirror (HBSY12, Thorlabs) was used to reflect the 532-nm beam and transmit the 1064-nm beam to a beam dump (LB2/M, Thorlabs). The 532-nm beam was then coupled and transmitted to the bifurcated optical fiber bundle (Cerampotec GmbH, Germany) through a pin-hole. A fraction of the 532-nm beam was used as a trigger to the clinical research US system (eCube 12R, Alpinion, South Korea) through a photodiode. The fiber bundle contains 1600 optical fibers (with a core diameter of 185 μm and a numerical aperture of 0.22), which were bifurcated in the middle to spread equally over two rectangles of area 4 cm \times 0.1 cm. The two rectangular fiber bundles and the L3–12 linear array imaging probe of the clinical US system are fitted into the slots of a custom 3-D printed (Dremel 3D20 3D printer, Singapore) probe holder to form the handheld probe. For image acquisition, the clinical research US system was used to acquire both PA and US beam-formed images. The frame rate of the system used was 5 Hz for both PA and US imaging modes. The L3–12 linear array transducer has 128 elements with

a center frequency of 8.5 MHz and 95% fractional bandwidth. The components were fixed in such a manner that the distance from tube (containing the blood clot) to transducer was \sim 1 cm and a light delivery angle of 10 deg was used.⁴⁴ At least 10 frames of each modality were saved before averaging to obtain the SNR values. The SNR is given in decibels (dB) as $\text{SNR} = 20 \times \log_{10}(V/n)$, where V is the signal amplitude and n is the mean of the background noise. Figure 1 shows the schematic representation of the experimental setup.

The width of the 532-nm beam was 7 mm and its light energy was \sim 100 mJ per pulse. Since the coupling and transmission efficiency of the fiber bundle was 25%, the fluence on the surface of the sample was calculated to be \sim 8.3 mJ/cm² (total area of illumination from both ends together is \sim 3 cm²). Thus, the fluence was well within the American National Standards Institute (ANSI) safety limit of 20 mJ/cm².⁴⁵

2.2 Sonothrombolysis

For sonothrombolysis, a 0.5-MHz spherically focused, single element, immersion transducer (A301S-SU, 1-in. diameter, 1.25-in. focus, Olympus) was used for the breakdown of the blood clots. A 10% duty cycle and an input voltage of 1 $V_{\text{peak-to-peak}}$ was delivered by a function generator (AFG3101, Tektronix Inc.). The function generator was connected to a radiofrequency (RF) amplifier (AG 1021, T&C Power Conversion, Inc.), which was operated at a gain of 55 dB and 300 W (amplification). A digital oscilloscope (TBS 1202B-EDU, Tektronix Inc.) was used to continuously monitor the voltages from the function generator and the RF amplifier during sonothrombolysis. A needle hydrophone with a sensitivity of 0.11 $\mu\text{V}/\text{Pa}$ was used to measure the pressure amplitude at the focus of the 0.5 MHz sonothrombolysis UST. For the ease of finding its focus, first a cone was 3-D printed (1-in. base diameter, vertex 1.25-in. from the base) such that the vertex of the cone represented the focus of the sonothrombolysis UST. The base of the cone was temporarily placed over the sonothrombolysis UST using transparent tape (Scotch Magic transparent tape, 3M, Singapore). Thereafter, the position of the needle hydrophone was carefully fixed such that the vertex of the 3-D printed cone was coincident with its needle. Prior to the pressure measurement, the cone was removed. The pressure amplitude of the sonothrombolysis UST was found to be 0.64 MPa.

2.3 Formation of Blood Clot

First, porcine blood was obtained from a local abattoir (Primary Industries Pte. Ltd., Singapore) in 200-mL Schott glass bottles (Sigma, Singapore) and immediately mixed with heparin at a concentration of 30 USP/mL of blood (Sigma, Singapore) after which it was transported to the university. For the blood clot formation, the heparinized blood was mixed with protamine sulfate⁴⁶ (Sigma, Singapore) at a concentration of 1 mg per 100 USP of heparin to reverse the effects of heparin. Thereafter, four parts of this blood was mixed with one part of 100 mM calcium carbonate (VWR, Singapore) followed by degassing for 3 min to get rid of the air bubbles. The blood was injected in a low-density polyethylene (LDPE) tube [outer diameter (OD) 4 mm and thickness 1 mm]. The tube was placed in a water bath at 37°C for 3 h. For stable clot formation, the tube containing the blood clot was then stored in a refrigerator at 8°C for 2 days prior to the experiment.

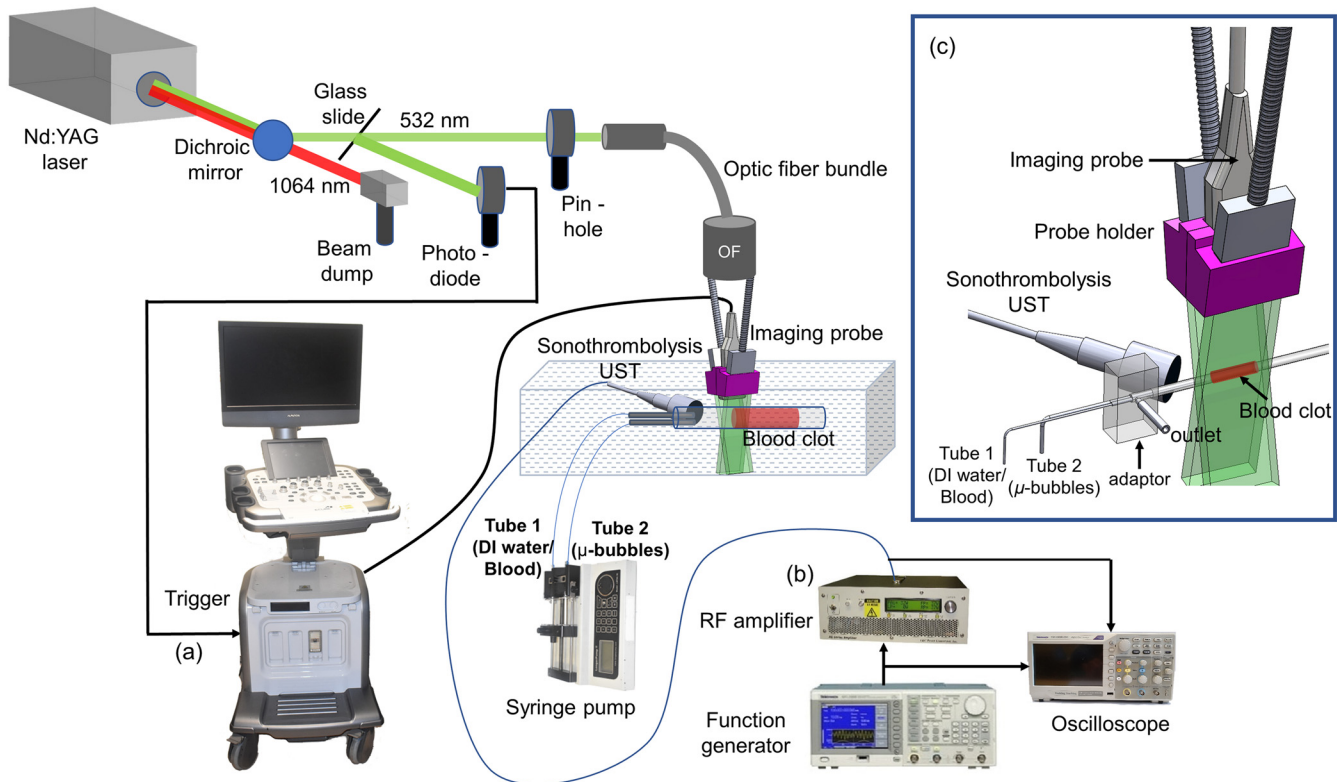


Fig. 1 Schematic representation (a) combined US and PA system for *in vitro* imaging, (b) setup for sonothrombolysis treatment, and (c) inset figure showing arrangement of the imaging US transducer and the sonothrombolysis transducer.

2.4 Generation of Microbubbles

A surfactant concentration of 5% PEG-40^{39,47} (Sigma Singapore) in addition to a fixed weight percentage of 10% and 10% of both glycerol (Sigma Singapore) and polypropylene glycol (Sigma Singapore) was taken in DI water. A clear solution is obtained after stirring it overnight at 1000 rpm using magnetic stirrer bars. About 5 mL of this solution is then poured in a beaker into which the rotor blades of a high shear homogenizer (DI60 Scilogex) are inserted. Simultaneously, an outlet from a perfluorobutane (PFB) gas cylinder (SynQuest Laboratories, Inc.) fitted with a gas pressure regulator (PGC-20L-60, Omega, Singapore) was connected to the beaker at a pressure of 10 psi. The rotor blades were then rotated at a constant speed of 12,400 rpm for 5 min to form the microbubbles.

After generating the PFB microbubbles, stability analysis of the microbubbles was done using optical microscopy. About 20 μ L of the surfactant solution was withdrawn from the beaker using a pipette and pushed out between two cover slips for observation under the microscope (Nikon Eclipse TE2000). The microscope was fitted with a CMOS camera (Phantom Miro ex4) for acquiring images at time $t = 0$ min [Fig. 2(a)] and at time $t = 30$ min [Fig. 2(b)] after generation of the microbubbles. ImageJ, an open source image processing program, was used for characterizing the stability of the microbubbles. A size distribution plot of the microbubbles was also obtained at time $t = 0$ min [Fig. 2(c)] and at time $t = 30$ min [Fig. 2(d)]. Initially, 45% of them were $<5 \mu\text{m}$ and 47.8% of the microbubbles were in the size range of 5 to 15 μm . After 30 min, only 14.2% of the microbubbles were $<5 \mu\text{m}$, whereas 52.1% of the microbubbles were in the size range of 7 to 13.5 μm .

Meanwhile, the total number of microbubbles was approximately reduced by half. The faster dissolution of the smaller microbubbles and the loss in the total number of microbubbles occur due to the Ostwald ripening phenomena.³⁹ Tables 1 [Fig. 2(c)] and 2 [Fig. 2(d)] show the mean diameter (μm), standard deviation (SD), and polydispersity index (PI) of the microbubbles at time $t = 0$ min and $t = 30$ min, respectively, after the formation of the microbubbles.

2.5 Delivery of “Microbubbles + DI Water” and “Microbubbles + Blood” to the Blood Clot

Two LDPE tubes, tubes 1 and 2, were inserted into the LDPE tube [OD 6 mm and thickness 1 mm] containing the blood clot. The thinner tube, tube 1 (OD 1.65 mm and thickness 0.25 mm) was used for the delivery of DI water initially, followed by heparinized blood for 10 min. It is to be noted that tubes 1 and 2 are quite flexible and could be easily inserted into the 6-mm OD tube. The thicker one, tube 2 (OD 2.42 mm, thickness 0.37 mm) was used for the delivery of the microbubbles throughout the experiment. The tube containing the blood clot and tubes 1 and 2 were immersed in a water tank. Also, tubes 1 and 2 were inserted into the blood clot-containing tube via an acrylic adaptor shown in Fig. 1(c). The adaptor also had an outlet tube for relieving the pressure in the blood clot-containing tube. These two tubes, tubes 1 and 2, were connected to a syringe pump (longer) at a flow rate of 0.08 mL/min.

3 Results and Discussion

For this work, the blood clot-containing tube was placed 1 cm below the US imaging probe in both US and PA modes. For

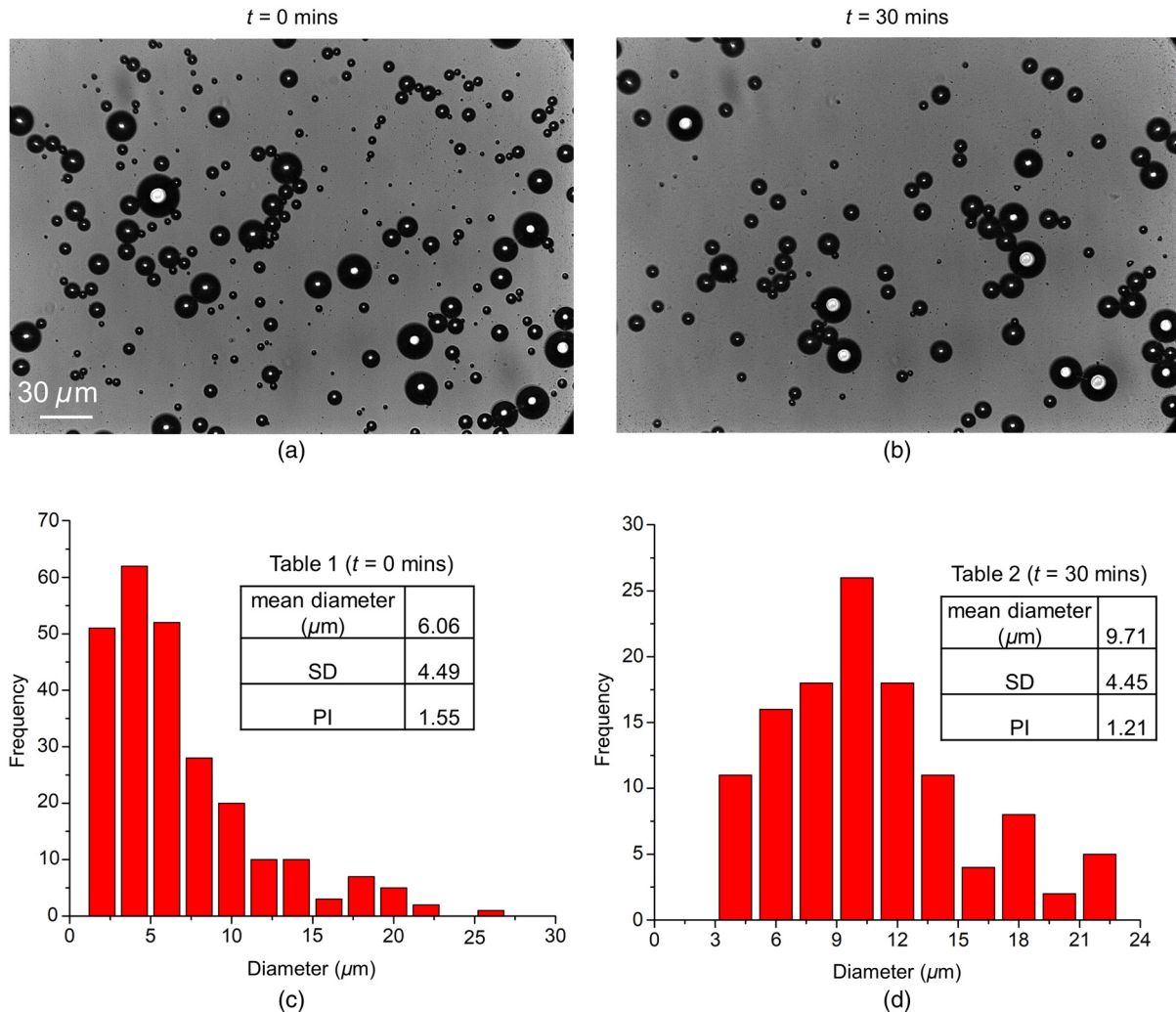


Fig. 2 Optical microscopy images showing microbubbles at time, (a) $t = 0$ min and (b) $t = 30$ min after generation. Size distribution (frequency vs diameter) of the microbubbles at time, (a) $t = 0$ min and (b) $t = 30$ min after generation. Tables 1 and 2 shows the mean diameter (μm), standard deviation (SD), and polydispersity index (PI) of the microbubbles at (c) time, $t = 0$ min and (d) $t = 30$ min, respectively.

future *in vivo* work, the light can be highly scattered if the blood vessel is deep in the tissue, which will weaken the PA signal. As the strength of the PA signal is proportional to the local laser fluence on the sample and the optical absorption, the local fluence will have to be increased to enhance the PA signal. Moreover, the increased scattering may give rise to artifacts, which can be removed by improving the reconstruction and data processing algorithm used. Earlier works have shown imaging depths exceeding 5 cm^{25,48} using similar combined US and PA imaging systems. In this work, experiments were first performed by injecting the DI water through tube 1 and microbubbles through tube 2 toward the blood clot. For imaging, the side of the blood clot facing the microbubbles was observed. Thereafter, sonothrombolysis was done for 30 min and, at every 10-min interval, US and PA images were taken. In the second part of the experiment, blood was injected through tube 1. Tube 2 was used for the delivery of microbubbles as before. A reflection artifact of the blood clot-containing tube's edge is seen as a horizontal line between the upper and the bottom boundaries of the tube in the blood clot region in the US signals throughout the experiment (Figs. 3–5). This is inherent to the clinical US

system (eCube) used in this work. These artifacts are difficult to remove at this point of time, as it requires access to the internal programming and settings of the program codes of the US machine.

Photos of the blood clot are shown in Fig. 3 before [Fig. 3(a)] and after [Fig. 3(b)] the injection of the microbubbles. In Figs. 3(a) and 3(c), DI water was present in both tubes 1 and 2. In Figs. 3(b) and 3(d), tube 1 is filled with DI water and tube 2 is filled with microbubbles. A fragment [Figs. 3(a)–3(c)] of the blood clot was visible along the lower edge of the LDPE tube between tubes 1, 2 and blood clot. After the injection of the microbubbles in the vicinity of the blood clot, this fragment of the blood clot was no longer visible [Fig. 3(d)] in the US mode at the bottom of the LDPE tube. This occurred due to the acoustic shadowing effect of the microbubbles as the acoustic waves are unable to penetrate the thick cloud of microbubbles.

Figure 4 shows the US and PA images of the blood clot in DI water + microbubbles at time $t = 0$ min [Figs. 4(a) and 4(c)] and time $t = 30$ min after administering sonothrombolysis treatment [Figs. 4(b) and 4(d)]. Figures 4(a) and 4(b) are in the US mode and Figs. 4(c) and 4(d) are in the PA mode. For PA

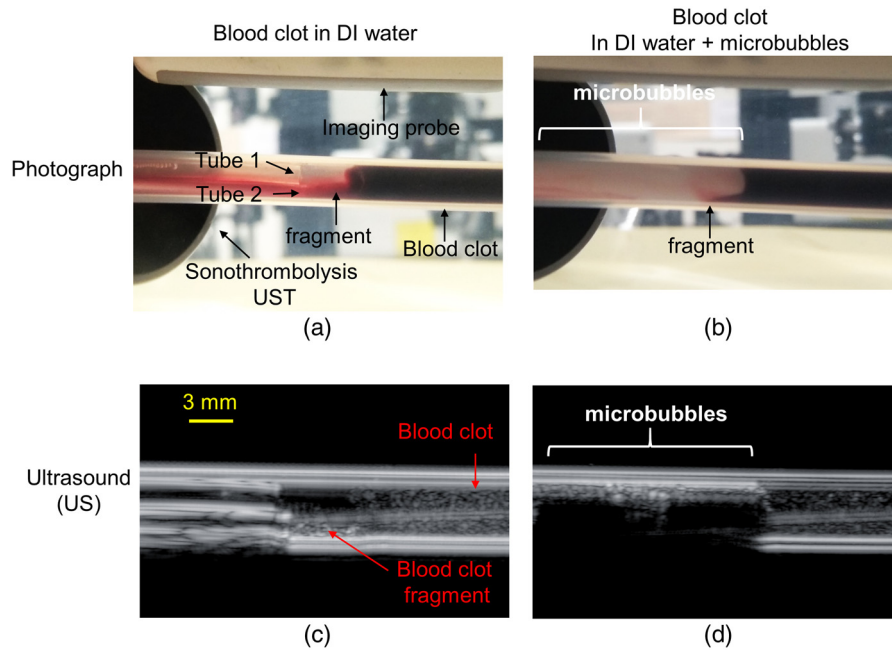


Fig. 3 Photographs showing LDPE tubes 1 and 2 inserted within the tube containing the blood clot in the (a) absence and (b) presence of microbubbles. (c) and (d) US images of the tubes containing the blood clot on the eCube system of (a) and (b) respectively. Blood clot fragment is visible in (a), (b), and (c).

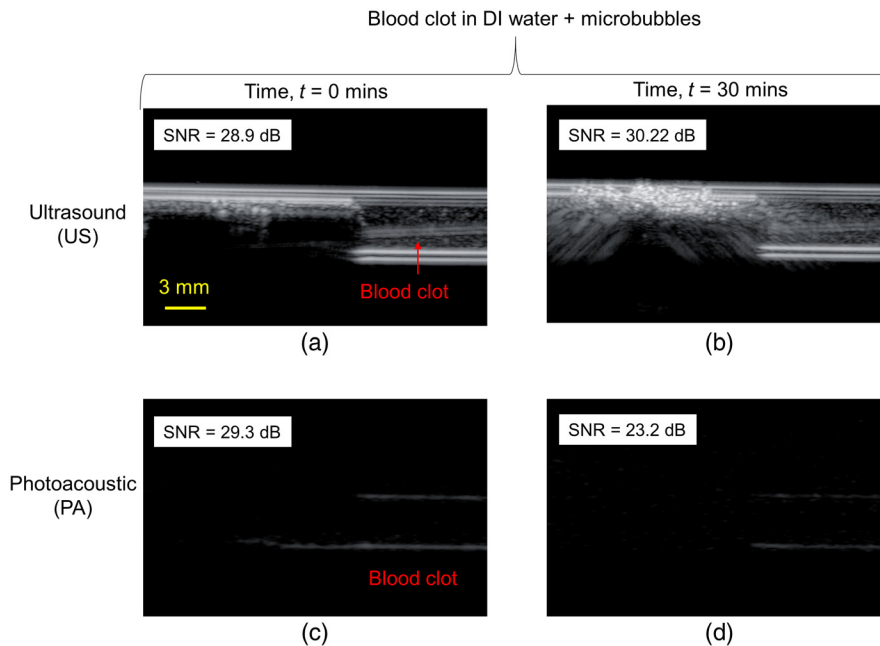


Fig. 4 *In vitro* images on the eCube system obtained from US and PA imaging modes where (a) and (c) show the blood clot in a tube filled with DI water + microbubbles at time $t = 0$ min before sonothrombolysis and (b) and (d) show the same blood clot after time $t = 30$ min of sonothrombolysis. The SNRs are shown for each figure.

imaging, 532-nm light excitation was chosen due to the strong absorption of light by blood at this wavelength. As mentioned previously, the fragment of the blood clot was not visible in the blood clot in the US mode, but when the PA mode was switched on, prominent PA signals were seen from both upper and lower edges of the blood clot, as shown in Fig. 4(c). PA signal was more pronounced along the lower edge than the upper one due to the presence of the fragment. US and PA SNR values of

the blood clot were 28.9 and 29.3 dB, respectively at time $t = 0$ min. Thereafter, the sonothrombolysis UST was turned on. At every 10-min interval, sonothrombolysis treatment was stopped and the US and PA images were recorded. Figures 4(b) and 4(d) show the US and PA images after 30 min of sonothrombolysis treatment. The US SNR value increased to 30.22 dB, whereas PA SNR value reduced to 23.2 dB. The US SNR value increased due to the softening of the blood clot as a result of

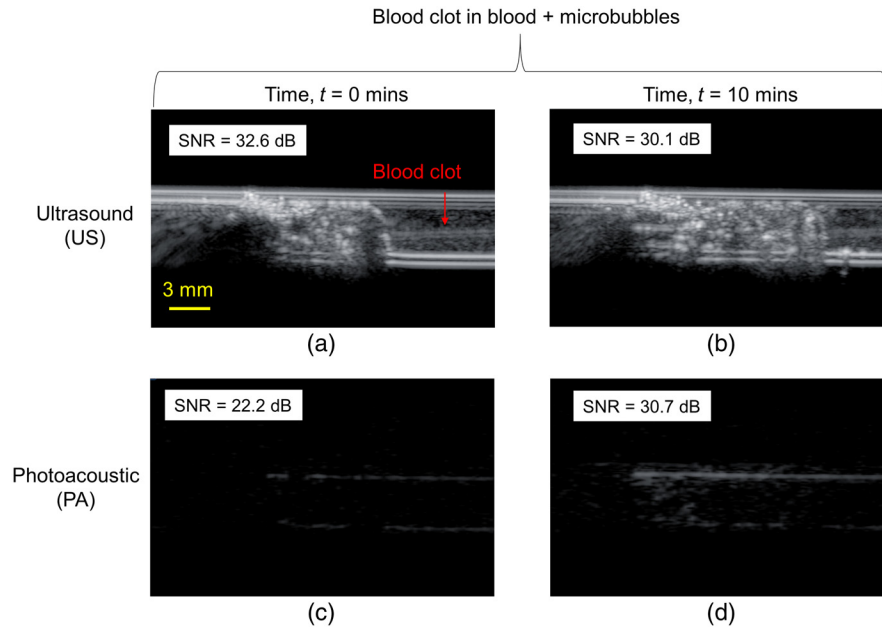


Fig. 5 *In vitro* images on the eCube system obtained from US and PAPA imaging modes where (a) and (c) show the blood clot in a tube filled with blood + microbubbles at time $t = 0$ min before sonothrombolysis and (b) and (d) show the same blood clot after time $t = 30$ min of sonothrombolysis. The SNRs are shown for each figure.

which microbubbles were able to penetrate it. As the microbubbles have a higher acoustic impedance, the US SNR values increased. The attrition of the blood clot was visible in the drop of the PA SNA value from 29.3 to 23.2 dB which reflected the wear and tear over time due to sonothrombolysis. In other words, the US SNR value increased by 4.6%, while the PA SNR values reduced by 20.8%.

Next, DI water was replaced by blood in tube 1 and the syringe pump was turned on until there were microbubbles + blood present in the vicinity of the blood clot. Figures 5(a) and 5(c) show the US and PA images at time $t = 0$ min. The US and PA SNA values of the blood clot were 32.6 and 22.2 dB, respectively. It must be noted that the blood used for microbubbles + blood contained heparin, because in its absence, the blood coagulates and cannot be pumped through the tubes. Even though blood clot contained protamine sulfate, additional injection of heparinized blood could overcompensate the structural integrity and shape of the blood clot. As a result, further softening of the blood clot took place and more microbubbles could penetrate it. Hence, the US SNR value increased to 32.6 dB [Fig. 5(a)] from 30.22 [Fig. 4(b)]. The PA SNR value remained relatively the same. Thereafter, the sonothrombolysis UST was turned on again. After 10 min, it was turned off and Figs. 5(b) and 5(d) shows the US and PA images after 10 min of sonothrombolysis treatment. Owing to the combined effect of heparin and sonothrombolysis, rapid degradation of the blood clot took place. As the blood clot partially dissolved, it got dislodged from its original location and was pushed back. The US SNR reduced slightly by 7.7% to 30.1 dB, whereas the PA SNR value increased by 38.8% to 30.7 dB. It was observed that the PA signal from the upper edge of the blood increases significantly from Figs. 5(c)–5(d). This occurred as microbubbles tend to float along the upper edge of the tube. As a result, more degradation took place along the upper edge of the blood clot, which resulted in greater penetration of the blood and microbubbles into the

blood clot. Hence, the PA signal was higher along the upper edge of the blood clot.

The change in the SNR values of the same blood clot is plotted in Fig. 6(a) over time. The (1) blue region shows the sonothrombolysis treatment in the presence of DI water + microbubbles and (2) yellow region shows the sonothrombolysis treatment in the presence of blood + microbubbles. At time $t = 0$ min, along the x -axis, the sonothrombolysis UST is off. Thereafter, it was turned on for 10 min and at 10-min interval; the sonothrombolysis UST was turned off for recording the images. In the presence of DI water + microbubbles, the US SNR values increase finally after fluctuating slightly.

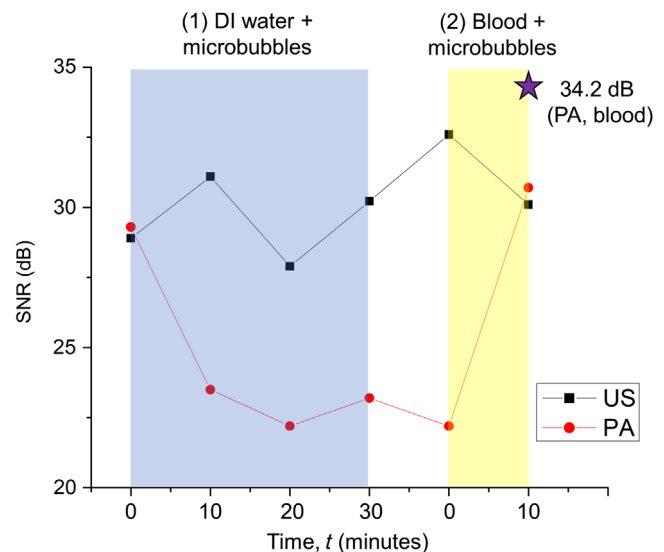


Fig. 6 Changes in the SNR values of the blood clot image over time. Region (1) DI water + microbubbles and region (2) blood + microbubbles.

Meanwhile, the PA SNR values dropped sharply in the first 10 min and then remained relatively constant. The clot degradation was fastest in the first 10 min only because initially the spherically focused UST which was used for sonothrombolysis had its treatment focus at the edge of the blood clot facing the microbubbles. As the blood clot degraded and receded beyond the focus, the pressure amplitude of the sonothrombolysis UST reduced due to which the degradation was much slower. Furthermore, when sonothrombolysis was done in the presence of blood + microbubbles; rapid degradation of the blood occurred due to the presence of heparin. Generally, heparin is an anticoagulant and is not used as a lytic drug. However, in this work, the blood clot was formed by adding protamine sulfate to heparinized blood. Hence, due to the additional presence of heparin, the blood clot lysed faster. After 10 min of sonothrombolysis treatment, the PA SNR value increased rapidly to 30.7 dB. The PA SNR of the tube filled with blood only is 34.2 dB. Owing to the presence of the microbubbles in the blood, it was still below this value.

The novelty of this work is that the potential of combined US and PA imaging was demonstrated during sonothrombolysis in a proof-of-concept study. A similar imaging setup can be used by other researchers to experiment with different kinds of microbubbles, controlled blood clots, etc. to do a more parametric study. Although US can provide information such as clot size and density, it does not provide any information regarding the composition of the blood clot and its surrounding fluids. Galanzha et al.³⁸ reported that RBC-rich clots have a positive PA contrast, RBC-depleted clots have a negative PA contrast, and mixed clots produce a pattern of both positive and negative contrasts. Assuming the clot used in this work was a mixed clot, it was observed that the PA SNR value of the blood clot was lower than that of blood. For a stronger PA signal, a higher laser fluence can be used. In this work, the fluence on the surface of the sample was calculated to be ~ 8.3 mJ/cm², which was well within the ANSI safety limit of 20 mJ/cm².⁴⁵ However, due to a possibility of damaging the fiber bundle and poor transmission efficiency of the fiber bundle (25%), the laser fluence was restricted to the current level, which resulted in a weaker PA signal from the blood.

PA imaging will be beneficial during sonothrombolysis treatment because during the DI water + microbubbles treatment, the PA signal dropped due to the degradation of the blood clot as expected. However, the PA SNR value increased rapidly during the blood + microbubbles treatment due to the combined effect of heparinized blood and sonothrombolysis. Hence, the rate of treatment progression had an opposite effect on the PA SNR values in the two cases: DI water + microbubbles and blood + microbubbles. This reversal in the trend of the PA SNR values is dependent on the changes in the local environment surrounding the blood clot. This provides much invaluable information in addition to the US images. PA imaging has been used for distinguishing chronic and acute blood clots,³⁶ erythrocyte-rich and platelet-rich clots,³⁸ monitoring the formation of blood clots during surgery,⁴⁹ etc., without the use of any exogenous contrast agents. It will also be beneficial to implement PA imaging during sonothrombolysis to observe the composition of the blood clot and the subsequent changes it undergoes noninvasively because the efficiency of the clot-dissolving drugs^{16,17} depends on the composition of the blood clot. Precise dosage of the clot-dissolving drugs is important because underdosage can increase the treatment duration, whereas overdosage can lead

to adverse effects such as hemorrhage. Since this is an *in vitro* proof-of-concept experiment performed in LDPE tubes, only the SNR values were analyzed to highlight the potential of combined US and PA imaging during sonothrombolysis. Further experiments will be done in future using *in vivo* animal models, which will reveal more information. It needs to be noted that DI water cannot be injected in large volumes into animal or patient during *in vivo* or clinical sonothrombolysis. In such a scenario, saline water ideally will have to be used. Since this work is only a proof-of-concept phantom study to explore the potential of combined US and PA imaging during sonothrombolysis treatment, DI water was used.

4 Conclusion

A combined US and PA imaging setup was used to determine the absolute changes in the composition of a porcine blood clot based on the changes in its local environment before and after microbubble-assisted sonothrombolysis. Two cases were studied: blood clot in DI water and blood clot in blood. As the same blood clot was used in this work, the US and PA SNR values were also comparable before and after sonothrombolysis for the two abovementioned cases. After 30 min of sonothrombolysis treatment in the presence of DI water + microbubbles, the US SNR increased by 4.6%, whereas the PA SNR value reduced by 20.8%. After 10 min of sonothrombolysis treatment in the blood + microbubbles experiment, the blood clot degraded much faster due to the presence of heparin in the blood and more microbubbles were able to penetrate the blood clot compared to the previous case. The US SNR value increased by 7.7% but the PA SNR value increased almost five times more by 38.3%. However, the final PA SNR value was still lower than the PA SNR value of pure blood due to the presence of the microbubbles in it.

Disclosures

The authors declare that there are no conflicts of interest related to this article.

Acknowledgments

The research was supported by a Tier 1 grant funded by the Ministry of Education in Singapore (RG144/18: M4012098). The authors would like to acknowledge Dr. Dinesh Kumar Chobey and Professor Zhou Yufeng from Nanyang Technological University, Singapore, for their help in measuring the pressure amplitude of the sonothrombolysis ultrasound transducer.

References

1. "Cardiovascular diseases (CVDs); 2017, <https://www.who.int/en/news-room/fact-sheets/detail/cardiovascular-diseases-cvds> (accessed 5 April 2019).
2. K. B. Bader, G. Bouchoux, and C. K. Holland, "Sonothrombolysis," in *Therapeutic Ultrasound*, J.-M. Escoffre and A. Bouakaz, Eds., pp. 339–362, Springer, Cham, Switzerland (2016).
3. S. Z. Goldhaber and H. Bounameaux, "Pulmonary embolism and deep vein thrombosis," *Lancet* **379**(9828), 1835–1846 (2012).
4. S. T. Roos et al., "Sonothrombolysis in acute stroke and myocardial infarction: a systematic review," *IJC Heart Vessels* **4**, 1–6 (2014).
5. A. J. Dixon et al., "In vitro sonothrombolysis enhancement by transiently stable microbubbles produced by a flow-focusing microfluidic device," *Ann. Biomed. Eng.* **46**(2), 222–232 (2018).
6. S. Kutty et al., "Microbubble mediated thrombus dissolution with diagnostic ultrasound for the treatment of chronic venous thrombi," *PLoS One* **7**(12), e51453 (2012).

7. J. Slikkerveer et al., "Ultrasound enhanced prehospital thrombolysis using microbubbles infusion in patients with acute ST elevation myocardial infarction: pilot of the sonolysis study," *Ultrasound Med. Biol.* **38**(2), 247–252 (2012).
8. A. T. Brown et al., "Microbubbles improve sonothrombolysis in vitro and decrease hemorrhage in vivo in a rabbit stroke model," *Invest. Radiol.* **46**(3), 202–207 (2011).
9. C. A. Molina et al., "Microbubble administration accelerates clot lysis during continuous 2-MHz ultrasound monitoring in stroke patients treated with intravenous tissue plasminogen activator," *Stroke* **37**(2), 425–429 (2006).
10. A. Nacu et al., "NOR-SASS (Norwegian Sonothrombolysis in Acute Stroke Study): randomized controlled contrast-enhanced sonothrombolysis in an unselected acute ischemic stroke population," *Stroke* **48**(2), 335–341 (2017).
11. A. Nacu et al., "A pragmatic approach to sonothrombolysis in acute ischaemic stroke: the Norwegian randomised controlled sonothrombolysis in acute stroke study (NOR-SASS)," *BMC Neurol.* **15**(1), 110–110 (2015).
12. E. T. Martin and D. A. Sandler, "MRI in patients with cardiac devices," *Curr. Cardiol. Rep.* **9**(1), 63–71 (2007).
13. M. V. Huisman and F. A. Klok, "Current challenges in diagnostic imaging of venous thromboembolism," *Blood* **126**(21), 2376–2382 (2015).
14. C. A. Molina et al., "Transcranial ultrasound in clinical sonothrombolysis (TUCSON) trial," *Ann. Neurol.* **66**(1), 28–38 (2009).
15. A. V. Alexandrov et al., "A pilot randomized clinical safety study of sonothrombolysis augmentation with ultrasound-activated perflutren-lipid microspheres for acute ischemic stroke," *Stroke* **39**(5), 1464–1469 (2008).
16. K. Kirchhof et al., "Does the result of thrombolysis with recombinant tissue-type plasminogen activator (rt-PA) in rabbits depend on the erythrocyte- and fibrin-content of a thrombus?," *RoFo: Fortschritte auf dem Gebiete der Rontgenstrahlen und der Nuklearmedizin* **176**(1), 98–105 (2004).
17. I. K. Jang et al., "Differential sensitivity of erythrocyte-rich and platelet-rich arterial thrombi to lysis with recombinant tissue-type plasminogen activator. A possible explanation for resistance to coronary thrombolysis," *Circulation* **79**(4), 920–928 (1989).
18. S. Z. Goldhaber and V. F. Tapson, "A prospective registry of 5,451 patients with ultrasound-confirmed deep vein thrombosis," *Am. J. Cardiol.* **93**(2), 259–262 (2004).
19. S. Atar et al., "Synergism of aspirin and heparin with a low-frequency non-invasive ultrasound system for augmentation of in-vitro clot lysis," *J. Thromb. Thrombol.* **15**(3), 165–169 (2003).
20. P. Singh, R. Kaur, and A. Kaur, "Clot composition and treatment approach to acute ischemic stroke: the road so far," *Ann. Ind. Acad. Neurol.* **16**(4), 494–497 (2013).
21. J. Minnerup and C. Kleinschnitz, "Visualization of clot composition in ischemic stroke: do we get what we see?," *Stroke* **42**(5), 1193–1194 (2011).
22. L. Lin et al., "Single-breath-hold photoacoustic computed tomography of the breast," *Nat. Commun.* **9**(1), 2352 (2018).
23. P. K. Upputuri and M. Pramanik, "Recent advances toward preclinical and clinical translation of photoacoustic tomography: a review," *J. Biomed. Opt.* **22**(4), 041006 (2017).
24. S. Manohar and D. Razansky, "Photoacoustics: a historical review," *Adv. Opt. Photonics* **8**(4), 586–617 (2016).
25. H. Ke et al., "Performance characterization of an integrated ultrasound, photoacoustic, and thermoacoustic imaging system," *J. Biomed. Opt.* **17**(5), 056010 (2012).
26. L. V. Wang and J. Yao, "A practical guide to photoacoustic tomography in the life sciences," *Nat Methods* **13**(8), 627–638 (2016).
27. L. V. Wang and S. Hu, "Photoacoustic tomography: in vivo imaging from organelles to organs," *Science* **335**(6075), 1458–1462 (2012).
28. J. Reber et al., "Non-invasive measurement of brown fat metabolism based on optoacoustic imaging of hemoglobin gradients," *Cell metabolism* **27**(3), 689–701 (2018).
29. C. L. Bayer et al., "Ultrasound-guided spectral photoacoustic imaging of hemoglobin oxygenation during development," *Biomed. Opt. Express* **8**(2), 757–763 (2017).
30. K. Sivasubramanian et al., "Near-infrared light-responsive liposomal contrast agent for photoacoustic imaging and drug release applications," *J. Biomed. Opt.* **22**(4), 041007 (2017).
31. M. Moothanchery et al., "In vivo studies of transdermal nanoparticle delivery with microneedles using photoacoustic microscopy," *Biomed. Opt. Express* **8**(12), 5483–5492 (2017).
32. W. Li and X. Chen, "Gold nanoparticles for photoacoustic imaging," *Nanomedicine* **10**(2), 299–320 (2015).
33. G. P. Luke, D. Yeager, and S. Y. Emelianov, "Biomedical applications of photoacoustic imaging with exogenous contrast agents," *Ann. Biomed. Eng.* **40**(2), 422–437 (2012).
34. K. Homan et al., "Prospects of molecular photoacoustic imaging at 1064 nm wavelength," *Opt. Lett.* **35**(15), 2663–2669 (2010).
35. D. Pan et al., "A facile synthesis of novel self-assembled gold nanorods designed for near-infrared imaging," *J. Nanosci. Nanotechnol.* **10**(12), 8118–8123 (2010).
36. A. B. Karpiouk et al., "Combined ultrasound and photoacoustic imaging to detect and stage deep vein thrombosis: phantom and ex vivo studies," *J. Biomed. Opt.* **13**(5), 054061 (2008).
37. M. A. Juratli et al., "Real-time label-free embolus detection using in vivo photoacoustic flow cytometry," *PLoS One* **11**(5), e0156269 (2016).
38. E. I. Galanzha et al., "In vivo flow cytometry of circulating clots using negative photothermal and photoacoustic contrasts," *Cytometry* **79**(10), 814–824 (2011).
39. D. Das et al., "On-chip generation of microbubbles in photoacoustic contrast agents for dual modal ultrasound/photoacoustic in vivo animal imaging," *Sci. Rep.* **8**(1), 6401 (2018).
40. K. Sivasubramanian et al., "Hand-held, clinical dual mode ultrasound-photoacoustic imaging of rat urinary bladder and its applications," *J. Biophotonics* **11**(5), e201700317 (2018).
41. K. Sivasubramanian, V. Periyasamy, and M. Pramanik, "Non-invasive sentinel lymph node mapping and needle guidance using clinical hand-held photoacoustic imaging system in small animal," *J. Biophotonics* **11**(1), e201700061 (2018).
42. K. Sivasubramanian and M. Pramanik, "High frame rate photoacoustic imaging at 7000 frames per second using clinical ultrasound system," *Biomed. Opt. Express* **7**(2), 312–323 (2016).
43. E. Stride and N. Saffari, "Microbubble ultrasound contrast agents: a review," *Proc. Inst. Mech. Eng.* **217**(6), 429–447 (2003).
44. K. Sivasubramanian et al., "Optimizing light delivery through fiber bundle in photoacoustic imaging with clinical ultrasound system: Monte Carlo simulation and experimental validation," *J. Biomed. Opt.* **22**(4), 041008 (2017).
45. "American National Standard for safe use of lasers," *ANSI Standard Z136.1-2007*, NY (2007).
46. S. Suelzu et al., "Impact of different dosage of protamine on heparin reversal during off-pump coronary artery bypass: a clinical study," *Heart, Lung and Vessels* **7**(3), 238–245 (2015).
47. M. Parhizkar, M. Edirisinghe, and E. Stride, "The effect of surfactant type and concentration on the size and stability of microbubbles produced in a capillary embedded T-junction device," *RSC Adv.* **5**(14), 10751–10762 (2015).
48. Y. Zhou et al., "A phosphorus phthalocyanine formulation with intense absorbance at 1000 nm for deep optical imaging," *Theranostics* **6**(5), 688–697 (2016).
49. M. A. Juratli et al., "Photoacoustic monitoring of clot formation during surgery and tumor surgery," *Proc SPIE* **8581**, 85814Q (2013).

Dhiman Das is currently a research fellow in the School of Chemical and Biomedical Engineering, Nanyang Technological University, Singapore. He received his PhD in chemical engineering from the same university in 2016. His research interests include the development and exploration of the potential applications of clinical photoacoustic systems, portable microfluidic systems, etc.

Manojit Pramanik is currently an assistant professor in the School of Chemical and Biomedical Engineering, Nanyang Technological University, Singapore. He received his PhD in biomedical engineering from Washington University in St. Louis, Missouri. His research interests include the development of photoacoustic/thermoacoustic imaging systems; image reconstruction methods; and clinical application areas, such as breast cancer imaging, molecular imaging, contrast agent development, and Monte Carlo simulation of light propagation in biological tissue.